Author Manuscript

Author Manuscript

Author Manuscript

Author Manuscript

HHS Public Access

Author manuscript

*Nat Neurosci*. Author manuscript; available in PMC 2011 July 01.

Published in final edited form as:

*Nat Neurosci*. 2011 January ; 14(1): 85–92. doi:10.1038/nn.2692.

# HCN Channelopathy in External Globus Pallidus Neurons in Models of Parkinson's Disease

**C. Savio Chan**[1], **Kelly E. Glajch**[1], **Tracy S. Gertler**[1], **Jaime N. Guzman**[1], **Jeff N. Mercer**[1,*], **Alan S. Lewis**[2], **Alan B. Goldberg**[1], **Tatiana Tkatch**[1,**], **Ryuichi Shigemoto**[3], **Sheila M. Fleming**[4], **Dane M. Chetkovich**[1,2], **Pavel Osten**[1,5], **Hitoshi Kita**[6], and **D. James Surmeier**[1]

[1] Department of Physiology, Northwestern University Feinberg School of Medicine, Chicago, IL 60611, USA

[2] Department of Neurology and Clinical Neuroscience, Northwestern University Feinberg School of Medicine, Chicago, IL 60611, USA

[3] Division of Cerebral Structures, National Institutes for Physiological Sciences, Myodaiji, Okazaki 444–8787, Japan

[4] Department of Psychology, University of Cincinnati, Cincinnati, OH 45221, USA

[5] Cold Spring Harbor Laboratory, Cold Spring Harbor, NY 11724, USA

[6] Department of Anatomy and Neurobiology, College of Medicine, The University of Tennessee Memphis, Memphis, TN 38163, USA

## Abstract

Parkinson's disease (PD) is a common neurodegenerative disorder characterized by a profound motor disability that is traceable to the emergence of synchronous, rhythmic spiking in neurons of the external segment of the globus pallidus (GPe). The origins of this pathophysiology are poorly defined. Following the induction of a parkinsonian state in mice, there was a progressive decline in autonomous GPe pacemaking that normally serves to desynchronize activity. The loss was attributable to the downregulation of an ion channel that plays an essential role in its generation – the HCN channel. Viral delivery of HCN2 subunits restored pacemaking and reduced burst spiking in GPe neurons. However, the motor disability induced by dopamine (DA) depletion was not reversed, suggesting that the loss of pacemaking was a consequence, not a cause, of key

Users may view, print, copy, download and text and data- mine the content in such documents, for the purposes of academic research, subject always to the full Conditions of use: http://www.nature.com/authors/editorial_policies/license.html#terms

Corresponding author: D. James Surmeier, Department of Physiology, Feinberg School of Medicine, Northwestern University, 303 E. Chicago Ave. Chicago, IL 60611 USA, j-surmeier@northwestern.edu, 312-503-4904.

*Department of Orthopaedic Surge ry, University of California, Irvine, CA 92868, USA;

**Istituto Italiano di Tecnologia, Via Morego, 30 16163 Genova, Italy.

AUTHOR CONTRIBUTIONS

C.S.C and D.J.S conceived the study, designed the experiments and directed the project. K.E.G and P.O. designed the viral expression strategy, generated and validated the HCN2 vectors *in vitro* and *in vivo*. C.S.C., T.S.G., J.N.G, J.N.M., and H.K. performed the recordings. A.S.L., R.S. and D.M.C. provided HCN mutants, generated the antibodies and performed the Western blots. C.S.C., A.B.G. and K.E.G. designed the probes and performed the qPCRs. T.T. participated in the exploratory phase of the qPCR experiments. K.E.G and S.M.F. performed the behavioral analyses. C.S.C. and D.J.S. wrote the paper. All authors discussed the results and implications and commented on the manuscript at all stages.

Author Manuscript Author Manuscript Author Manuscript Author Manuscript

network pathophysiology – a conclusion consistent with the ability of L-type channel antagonists to attenuate silencing following DA depletion.

Parkinson's disease (PD) is a common, progressive, debilitating neurodegenerative disorder whose motor symptoms include bradykinesia, rigidity and resting tremor [1–3]. These symptoms are attributable to the loss of dopaminergic neurons in the substantia nigra pars compacta (SNc). Although the principal target of this innervation is the striatum, the most prominent pathophysiology in animal models of late stage PD and in human patients occurs in one of its synaptic targets, the external segment of the globus pallidus (GPe; also called just the globus pallidus in rodents). In healthy animals, the autonomous, high discharge rate of GPe neurons is episodically interrupted by pauses created by convergent activity in GABAergic striatopallidal neurons involved in action selection and procedural motor learning [4, 5].

The autonomous and somewhat variable pacemaking of GPe neurons helps to keep their activity un-correlated from that of their neighbors, allowing the basal ganglia microcircuits they are part of to function independently in movement control [6–9]. In late stage PD, this activity pattern changes dramatically. In this state, GPe neurons and synaptically-coupled neurons in the subthalamic nucleus (STN) begin to spike in synchronous, high frequency bursts [1–3, 10–12]. This pathological pattern is reversed by therapeutically effective doses of L-DOPA or by high frequency deep brain stimulation (DBS) of the STN – establishing a causal linkage between it and the core motor symptoms of PD [1–3].

In spite of its importance, the origins of this network pathophysiology are unclear. In the PD state, the loss of DA is thought to disinhibit striatopallidal medium spiny neurons (MSNs), leading to the suppression of autonomous activity in GPe neurons and emergence of rhythmic bursting in the network they form with the STN. The problem with this scenario is that although striatopallidal MSNs are more excitable following DA depletion [13], they are not tonically active as demanded by the modeling work [14, 15]. The other obvious possibility is that the decorrelating, autonomous activity of GPe neurons is lost in PD, mimicking a sustained GABAergic inhibition. To test this hypothesis, GPe neurons from rodent PD models were examined. These studies revealed that, indeed, DA depletion produced a progressive loss of autonomous pacemaking in GPe neurons. The loss was attributable to the selective downregulation of an ion channel that plays an essential role in the generation GPe pacemaking – the hyperpolarization and cyclic nucleotide-gated (HCN) channel [6, 16, 17]. However, restoration of pacemaking by viral delivery of an HCN channel construct failed to alleviate the motor disability following DA depletion – suggesting that the primary network defect resided elsewhere and the channelopathy in GPe neurons was a maladaptive form of homeostatic plasticity. In agreement with this hypothesis, antagonism of L-type $Ca^{2+}$ channels, which are key regulators of calcium entry during pathological burst spiking in GPe neurons and homeostatic plasticity in other neurons [18, 19], significantly attenuated the loss of autonomous activity following DA depletion.

Author Manuscript Author Manuscript Author Manuscript Author Manuscript

# RESULTS

## Autonomous pacemaking in GPe neurons is lost in PD models

The impact of lesioning SNc DA neurons initially was assessed with electrophysiological approaches in brain slices from mice that had stereotaxic injections of the toxin 6-hydroxydopamine (6-OHDA). One week after lesioning, roughly 60% of GPe neurons had lost their normally robust autonomous pacemaking; of those still pacemaking, over a third had significantly lower than normal discharge rates (Fig. 1a). Similar results were obtained following treatment with the broad spectrum inhibitor of vesicular monoamine transporter (reserpine) or following treatment with an inhibitor of DA synthesis (α-methyl-tyrosine) – both of which induce parkinsonism in mice (Fig. 1a). In contrast, disrupting the synthesis of another amine – serotonin – by treating mice with DL-*p*-chlorophenylalanine methyl ester hydrochloride had no effect on the autonomous activity of GPe neurons (n = 8, data not shown).

To determine whether silencing was a transient phenomenon, GPe neurons were examined 3–4 weeks following 6-OHDA lesioning of the ascending DA pathway. At these time points, a large fraction of GPe neurons remained silent (Fig. 1b, left). The silencing at this time point was all-or-none (Fig. 1b, middle). Because variability in the extent of the lesion could contribute to variation in the extent of silencing, animals were behaviorally assayed using a limb asymmetry test that has been correlated with lesion magnitude [20], [21]. Assessment of autonomous activity in GPe neurons in brain slices from these mice revealed a clear correlation between degree of silencing and the severity of the behavioral deficit (Fig. 1b, right).

Next, GPe neurons were examined *in vivo*. Rats were subjected to unilateral 6-OHDA lesioning, as with mice described above. Four to six weeks later, animals were anesthetized and single GPe neurons recorded using extracellular electrodes. In contrast to the situation in brain slices, GPe neurons were spiking at close to the same rate found in control animals (Fig. 2a–b). To determine whether this activity was autonomously generated or dependent upon excitatory synaptic input from the STN, the $GABA_A$ receptor agonist muscimol was injected into the STN while recording from GPe neurons. Muscimol injection into the STN consistently suppressed cortically-evoked, short latency excitatory responses in GPe neurons that depend upon an STN relay, demonstrating that the manipulation had effectively shut down the STN (Fig. 2c). Normally, the suppression of STN activity only modestly reduced GPe spiking (Fig. 2a–b, left); but, in the 6-OHDA lesioned animal, silencing the STN with muscimol silenced GPe neurons (Fig. 2a–b, right), arguing that, as seen in brain slices, the capacity of GPe neurons to autonomously spike was lost.

## Silencing was not dependent upon striatopallidal GABA release

What was responsible for the loss of autonomous activity in the PD models? One consequence of DA depleting lesions is the disinhibition of GABAergic striatopallidal MSNs [1], [22]. This disinhibition occurs not only in the somatodendritic region of striatopallidal MSNs, but also at the GABAergic terminals synapsing on GPe neurons [23], [24]. In simulations, an increased tonic release of GABA onto GPe neurons is capable of

Author Manuscript Author Manuscript Author Manuscript Author Manuscript

hyperpolarizing them enough that autonomous pacemaking is suppressed [14], [15]. If enhanced GABA release at striatopallidal terminals was responsible for silencing, antagonizing $GABA_A$ receptors should restart pacemaking. However, application of the $GABA_A$ receptor antagonist SR95531 (10 μM) did not restart pacemaking in GPe neurons in brain slices from DA depleted mice (n = 18). Antagonizing $GABA_B$ receptors with CGP55845 (1 μM, n = 6) or blocking their target, the Kir3 channel, with $Ba^{2+}$ (500 μM, n = 6), also failed to restart pacemaking. Lastly, even in GPe neurons that were not silenced following DA depletion (n = 10), the rate of autonomous activity was not altered by antagonism of $GABA_A$ receptors (Fig. S1), demonstrating that tonic elevation of GABA release was not a factor in silencing of GPe neurons, at least *in vitro*.

## HCN channel currents were reduced in PD models

In GPe neurons, HCN and Nav1 $Na^+$ channels generate the inward current required to sustain pacemaking, ensuring that the axosomatic membrane voltage does not have a stable point [6], [16], [17]. When the membrane potential repolarizes after a spike, HCN channels open and allow cations to flow into the cell, depolarizing the membrane potential into the voltage range where $Na^+$ channels become active; activation of $Na^+$ channels then brings the membrane potential to spike threshold, completing the pacemaking cycle.

Voltage-clamp recordings from acutely isolated GPe neurons failed to find any downregulation of $Na^+$ channel currents following DA depletion (Fig. S2). Corroborating this result, there was no consistent change in the expression of voltage-gated $Na^+$ channels ($Na_v1.1$, $Na_v1.2$ and $Na_v1.6$) or $Na^+$ leak channels (Nalcn/UNC-80) by DA depletion in tissue (data not shown) and single-cell level PCR assays (Fig. S2). Moreover, intracellular current injection into silenced GPe neurons evoked a normal pattern of spiking (Fig. S3), suggesting that the deficit produced by DA depletion was not attributable to a downregulation in $Na^+$ channel density or function.

In contrast, several lines of physiological evidence pointed to a downregulation in HCN channel function. First, the resting membrane potential of silenced neurons was relatively hyperpolarized (Fig. 3ab), averaging ~−63 mV (n = 20); this is roughly 10 mV more negative than that of naïve GPe neurons made quiescent by blocking $Na^+$ channels with tetrodotoxin (TTX) [17], suggesting that the normal depolarizing influence of HCN channels had been reduced by DA depletion. Second, negative current pulses delivered to the soma were much more effective in hyperpolarizing the membrane in silenced neurons than in naïve GPe neurons or in GPe neurons that retained autonomous activity (Fig. 3a–b). To more directly measure HCN channel currents, voltage-clamp measurements were made with a standard two-step protocol [6], [25]. In GPe neurons from mice treated for 5 days with reserpine, peak HCN currents were cut in half (Fig. 3c). Furthermore, the amplitudes of the HCN channel currents measured in voltage clamp were strongly correlated with the magnitude of the hyperpolarization produced by current steps in the same cell (Fig. 3d). The same reduction in HCN channel currents was found in GPe neurons from mice chronically (3–4 weeks) DA depleted by 6-OHDA injection into the medial forebrain bundle (Fig. 3f–g), demonstrating the commonality of the phenomenon across PD models.

Author Manuscript Author Manuscript Author Manuscript Author Manuscript

## HCN channel expression was downregulated in PD models

One of the ways to downregulate HCN channel currents is to diminish the allosteric enhancement of channel opening produced by modulators like cAMP (cyclic adenosine monophosphate) or $PIP_2$ (phosphatidylinositol 4,5-bisphosphate) [26]. A hallmark of this type of modulation is a shift in the voltage dependence of activation and acceleration in gating. However, there was no difference in the voltage-dependence of HCN channels in GPe neurons (Fig. 3e–f) from DA depleted mice (median half-activation voltage: naïve = −90.1 mV, n = 5; reserpine = −87.4 mV, n = 12; 6-OHDA = −92.5 mV, n = 8; P>0.05, Mann-Whitney). Furthermore, HCN channel gating was not altered by DA depletion. With a voltage step to −130 mV, the growth of HCN channel currents had fast and slow components (consistent with our earlier observations) [6]; DA depletion did not significantly change the time constant (Fig. S4) of either component (median $\tau_{fast}$: naïve = 167, n = 20; reserpine = 189, n = 25; median $\tau_{slow}$: naïve = 937 ms, n = 20; reserpine = 924 ms, n = 25; P>0.05, Mann-Whitney). Despite substantial space-clamp constraints inherent in these measurements, they suggest that intracellular modulation is unlikely to be altered following DA depletion.

Another way to decrease HCN channel currents is to decrease surface expression. To test this hypothesis, GPe (and cerebral cortex) membrane fractions were used for Western blot analyses. DA depletion decreased the abundance of all four HCN α-subunits (HCN1–4) in GPe tissue, but did not alter expression in the cerebral cortex (Fig. 4a). In addition, DA depletion modestly downregulated GPe expression of the tetratricopeptide repeat (TPR)-containing Rab8b-interacting protein (TRIP8b), the HCN channel β-subunit in the brain [27], [28]. To determine whether the drop in expression of HCN channels was a consequence of transcriptional regulation or altered trafficking, quantitative real-time PCR (qPCR) was used to estimate mRNA levels (Fig. 4b). In agreement with previous work [6], [29], this analysis revealed that HCN2 mRNA is enriched in the GPe (~2.5 times higher than in total brain). More importantly, DA depletion with reserpine induced a significant reduction in the abundance of all four HCN subunit mRNAs, as well as TRIP8b mRNA (Fig. 4b). The drop in HCN and TRIP8b mRNA also was sustained 3–4 weeks after a 6-OHDA lesion (Fig. S5).

## Viral delivery of HCN2 restored pacemaking but not motor disability

Although the strong correlation between silencing and downregulation of HCN channel expression suggests a causal linkage, it is not unequivocal evidence. If there is a causal linkage, downregulating HCN expression without depleting DA should silence GPe neurons. Application of the HCN channel antagonist ZD7288 or $Cs^+$ suppresses autonomous activity in naïve GPe neurons [6]. The problem with the interpretation of this result is that these blockers are known to have effects on other ion channels that might influence pacemaking. As shown above, the predominant HCN subunit in GPe neurons is the HCN2 subunit. If DA depletion silences GPe neurons principally by downregulating transcription of the HCN2 gene, then the absence of the HCN2 transcript should mimic DA depletion. To test that hypothesis, HCN2 null mice [30] were examined along with HCN1 null mice [31]. In mice lacking HCN1 subunits, HCN channel current amplitude was normal, as was the rate of pacemaking (Fig. 5, P>0.05, Mann-Whitney). In contrast, GPe neurons from HCN2 null mice had significantly reduced HCN channel currents and were completely silent (Fig. 5).

Author Manuscript Author Manuscript Author Manuscript Author Manuscript

To provide an additional test of the hypothesis that HCN channel downregulation was responsible for DA depletion induced silencing, HCN2 subunits were reintroduced into GPe neurons three weeks after near complete unilateral lesions of DA neurons with 6-OHDA. This was accomplished by stereotaxic injection into the GPe of adeno-associated virus (AAV) carrying an HCN2 subunit expression construct (Fig. 6a–b, S6). Two to five weeks after virus injection, pacemaking was restored in the majority (9 of15) of infected GPe neurons recorded in brain slices, whereas neighboring uninfected GPe neurons remained silent (n = 5, Fig. 6c–d). To verify that HCN2 delivery would have a similar impact *in vivo*, unilaterally 6-OHDA lesioned rats were injected with the same AAV vector and GPe activity sampled three weeks later using extracellular recording *in vivo*. As predicted from the *in vitro* assays, basal discharge rate was increased (median rate: lesion = 24.8 Hz, n = 113; lesion+virus = 30.8 Hz, n = 111; $P<0.001$, Mann-Whitney) and bursting decreased (median burst index: lesion = 0.49, n = 113; lesion+virus = 0.36, n = 111; $P<0.001$, Mann-Whitney) in GPe neurons from rats treated with the HCN2-AAV (Fig. 6e).

If the loss of autonomous activity was the primary cause of the pathological rhythmic bursting underlying the motor disability seen following DA depletion, then its restoration with the HCN2-AAV should ameliorate the disability. However, AAV-mediated HCN2 delivery to unilaterally lesioned mice failed to significantly improve ipsilateral forepaw usage, open field activity or other sensorimotor functions (Fig. S6). This failure did not appear to be a consequence of an inability to infect a large population of GPe neurons, as even robust infections (e.g. Fig. 6b–c) did not lead to amelioration of motor deficits ($P>0.05$, Mann-Whitney).

## Antagonism of L-type $Ca^{2+}$ channels mitigated silencing

The failure of HCN2 up-regulation and restoration of autonomous pacemaking in GPe neurons to alleviate DA depletion-induced motor deficits argues that it is not the cause of the network pathology underlying the deficits, but rather an effect. This conclusion is consistent with recent work showing that inactivating the DA projection to the basal ganglia induces pathological rhythmic bursting in GPe neurons in minutes, not days [32]. In many neurons, a significant perturbation in spiking triggers the induction of homeostatic mechanisms in an attempt to restore normal activity [18], [19]. Although synaptic scaling is the best-studied form of homeostatic plasticity, intrinsic mechanisms, like ion channel expression, have also been identified as homeostatic targets [18], [19]. In both cases, $Ca^{2+}$ entry through L-type channels or NMDA receptors serves as a homeostatic control variable. Following DA depletion, the most prominent change in the activity of GPe neurons is not in mean spike rate but in emergence of rhythmic spike bursts (e.g. Fig. 2). For this perturbation to trigger homeostatic mechanisms aimed at decreasing spiking, spike bursts should significantly increase $Ca^{2+}$ entry through L-type channels. To test this hypothesis, the intracellular concentration of $Ca^{2+}$ was monitored in GPe neurons using the $Ca^{2+}$ indicator Fluo-4 and two photon laser scanning microscopy (2PLSM). During normal pacemaking there was no detectable spike-dependent fluctuation in intrasomatic or intradendritic $Ca^{2+}$ concentration (Fig. 7a–c). However, evoking a burst of spikes transiently elevated cytosolic $Ca^{2+}$ concentration and a large component of this rise was attributable to opening of L-type channels, particularly in dendritic regions (Fig. 7a–c).

Author Manuscript Author Manuscript Author Manuscript Author Manuscript

To test the hypothesis that burst-evoked opening of L-type $Ca^{2+}$ channels triggered the downregulation of HCN channels, mice were treated with isradipine, a blood-brain barrier penetrant L-type $Ca^{2+}$ channel antagonist [25], during the course of DA depletion. Consistent with this hypothesis, the firing rate of GPe neurons from mice treated with isradipine was significantly higher than that in neurons from control mice (median rate:reserpine alone = 0 Hz, n = 55; reserpine & isradipine = 10.34 Hz, n = 22; $P<0.05$, Mann-Whitney) (Fig. 7d–e). Isradipine significantly shifts the firing rate of GPe neurons from the DA depleted animals toward that seen in naïve animals ($P<0.05$, Kolmogorov-Smirnov).

## DISCUSSION

Our results show that rendering rodents parkinsonian by DA depletion induces the downregulation of HCN channel expression in GPe neurons, leading to a loss of their characteristic autonomous pacemaking. The loss of autonomous activity was progressive, encompassing more of the GPe neuronal population in the days following DA depletion. Viral delivery of an HCN2 subunit expression construct restored pacemaking and reduced pathological rhythmic burst spiking of GPe neurons of PD models. Systemic administration of an L-type $Ca^{2+}$ channel antagonist that crosses the blood-brain barrier also mitigated the adaptation, suggesting that it reflected a maladaptive form of homeostatic plasticity.

### HCN channels and the origins of rhythmic bursting in PD models

HCN channels are necessary for autonomous spiking in GPe neurons, as they keep the membrane potential from stabilizing below the activation threshold for voltage-dependent $Na^+$ channels [6, 17]. Sustained DA depletion reduced HCN channel currents in GPe neurons. This was paralleled by a reduction in all four of the pore-forming HCN subunits at both the mRNA and protein levels. TRIP8b, an HCN trafficking protein, was also downregulated. The downregulation of the GPe dominant HCN2subunit was the most prominent of these changes. Selective deletion of the gene coding for HCN2 (but not HCN1) also silenced GPe neurons and viral-delivery of an HCN2 expression construct restored pacemaking following DA depletion – firmly establishing the causal linkage between HCN2 downregulation and loss of pacemaking.

As outlined above, in PD models and in late stage PD patients, GPe and STN neurons spike in synchronous, rhythmic bursts – a behavior that is rarely seen in healthy brains [1–3, 10–12]. This pathophysiological activity is correlated with motor symptom severity and is responsive to L-DOPA treatment, suggesting it is causally linked to motor dysfunction [33]. Because of its linkage to the core PD symptoms, its origins have been the subject of a great deal of speculation. Because the GPe and the STN are a reciprocally connected pair of excitatory and inhibitory cell groups [10], the dyad they form seems perfectly designed to produce alternating periods of activity and quiescence, or rhythmic bursting. With the widespread and potent axonal projection of GPe neurons [10], this activity pattern could entrain many basal ganglia nuclei [34] leading to global network synchrony and the motor symptoms of the disease. What is puzzling is why this network does not exhibit rhythmic bursting normally. Simulations have shown that there are several factors controlling this behavior, including network structure, connectivity and ongoing autonomous activity in GPe

Author Manuscript Author Manuscript Author Manuscript Author Manuscript

neurons [14], [15]. In simulations, pathological rhythmic bursting can be triggered by modestly hyperpolarizing GPe neurons with a tonic striatal GABAergic input, effectively suppressing decorrelating, autonomous activity. Although a deficit in pacemaking might mimic this situation and induce rhythmic bursting, there are several reasons why this is an unlikely scenario in PD models. First, the loss of autonomous pacemaking takes days to evolve following DA depletion, whereas rhythmic bursting takes minutes to appear following pharmacological inactivation of DA fibers [32]. Second, the restoration of pacemaking by viral HCN2 gene delivery to the GPe *in vivo* did not reverse the motor consequences of DA depletion and only attenuated rhythmic bursting.

If rhythmic bursting does not originate in the loss of pacemaking in GPe neurons, then where? Striatopallidal GABAergic MSNs are a major regulator of GPe activity. Disinhibition of these MSNs following DA depletion has long been thought to be a key part of the pathophysiology of PD [1], [22]. By increasing MSN responsiveness to cortical excitation and by diminishing inhibitory presynaptic regulation of their GABA release within the GPe, DA depletion is thought to potentiate the ability of corticostriatal networks to inhibit GPe neurons [34]. Release from an intense inhibitory MSN barrage could induce rebound burst spiking in GPe neurons. However, a more likely possibility given the intermittent nature of MSN activity (even in PD models) is that bursting is driven by the STN. The STN provides a robust excitatory synaptic input to GPe neurons that is altered in PD models. In unilateral 6-OHDA models, the cerebral cortex and the STN frequently oscillate in synchrony and this oscillation propagates into the network formed by the STN and GPe [34], [35]. One way of testing this hypothesis would be to ablate the STN input prior to DA depletion. If STN bursting was critical to the adaptation in GPe, this should prevent the downregulation of HCN subunits.

### Rhythmic bursting, pacemaking and homeostatic plasticity

If the loss of pacemaking does not cause rhythmic bursting, could rhythmic bursting cause the loss of pacemaking? In other neurons, HCN channels are downregulated following sustained elevations in excitatory synaptic input. In models of epilepsy, for example, HCN subunit expression is downregulated in entorhinal cortex or hippocampal neurons following kindling [36]–[38]. This appears to be a form of homeostatic plasticity intended to return spiking rate to a pre-determined set-point [18], [19], [39]. Although the mean spiking rate of GPe neurons does not change consistently following DA depletion, an increased incidence of burst spiking might be mis-interpreted by the cellular machinery controlling homeostatic plasticity as an increase in mean rate. $Ca^{2+}$ entry though L-type channels typically serves as a surrogate measure of spiking [40]. In GPe neurons, the $Ca^{2+}$ signal attributable to influx through L-type channels was dramatically enhanced by burst spiking. In keeping with the hypothesis that influx of $Ca^{2+}$ through L-type channels during bursting triggered homeostatic downregulation of HCN channel expression, systemic administration of the L-type channel antagonist isradipine attenuated the loss of pacemaking. Although L-type $Ca^{2+}$ channels are widely distributed, the most likely site of action was the GPe neuron itself where pacemaking keeps the membrane potential in a range where the affinity of these channels for dihydropyridines is the highest [41]. Another potential contributor to the

Author Manuscript Author Manuscript Author Manuscript Author Manuscript

adaptation seen in GPe neurons, and one that is known to contribute to other forms of homeostatic plasticity [19], is the NMDA receptor.

Although the downregulation of HCN channels does not induce rhythmic bursting, it might exacerbate it. Normally, deactivation of HCN channels creates an opposing hyperpolarizing current that diminishes the impact of a sustained excitatory synaptic barrage [42]. Downregulating membrane HCN channels should remove this dendritic brake and enhance the ability of repetitive STN spiking to evoke burst spiking in GPe neurons. This could be similar to the situation in the hippocampus where HCN downregulation renders neurons more susceptible to high frequency, repetitive synaptic input, increasing seizure severity [36–38]. This tendency should be increased further by the loss of presynaptic $D_2$ receptor inhibition of glutamate release [43], as well as possible unblocking of postsynaptic of NMDA receptors [44]. Thus, the homeostatic response of GPe neurons appears to be maladaptive in that it promotes the pattern of discharge that is most disruptive to the rest of the network and to motor control. If this were the case, attenuating this adaptation could prove beneficial to late stage PD patients when used in conjunction with other therapies.

## METHODS

### Animals

Male C57BL/6 mice (Charles River), homozygous HCN1 null mice [31] (*Hcn1*$^{-/-}$, The Jackson Laboratory), homozygous HCN2 null (*Hcn2*$^{ap/ap}$, *apathetic*) mice [30], and Sprague Dawley rats (Charles River) were used in this study. The handling of animals and all procedures were conducted in strict accordance with a protocol approved by institutional Animal Care and Use Committees, and were in compliance with the NIH Guide to the Care and Use of Laboratory animals.

### Acute dopamine depletion in mice

Acute DA depletion was produced by unilateral lesions of the nigrostriatal system by terminal field (i.e. caudate putamen) injection of 6-hydroxydopamine (6-OHDA). Male C57BL/6 mice at postnatal day 18–20 were anesthetized, 6-OHDA was dissolved at a concentration of 2.5–5 μg/μl saline with 0.2 μg/μl ascorbic acid and injected in final dosages of 4–15 μg). 6-OHDA injection (1–1.5 μl) was performed using a calibrated glass micropipette. Electrophysiological experiments were performed 6–8 days later. Alternatively, acute DA depletions were produced in C57BL/6 mice, aged postnatal day 17 to 25, by administering the indole alkaloid reserpine (5 mg/kg, i.p.) for 5 successive days. The mice were killed for experiments 2–4 h after the final injection. Partial DA depletion was achieved with α-methyl-DL-tyrosine methyl ester hydrochloride (α-MT) with three daily i.p. injections of 100 mg/kg.

### Isradipine treatment

Isradipine (0.5 mg/kg) was injected into animals twice a day at a 12-hr interval during the course of reserpine treatment. Animals were then sacrificed 12 hours after the last injection. Autonomous firing of GPe neurons was assessed *in vitro*.

Author Manuscript Author Manuscript Author Manuscript Author Manuscript

### Chronic dopamine depletion in mice and rats

Chronic DA depletion in mice (postnatal day 21–28) was accomplished by injection of 6-OHDA into the medial forebrain bundle with procedure similar to above. Mice were sacrificed for recordings 3–4 weeks postoperative. Rats (200–250 g) were anesthetized, placed in a stereotaxic apparatus and unilaterally injected with (6-OHDA; 2 μg/μl of saline containing 0.1% ascorbic acid) into the ascending mesotelencephalic DA-bundle. The animals were allowed to recover from the surgery for at least two weeks. To assess the degree of DA depletion in rodents, the cylinder test was used to quantify impairment in forelimb usage after 6-OHDA injections [20], [21]. Contacts made by each forepaw on the wall of a clear glass cylinder (9 cm wide for mice; 19 cm wide for rats) were scored from videotapes by an observer blind to the animal's identity. The number of spontaneous exploratory forelimb touches were recorded for each animal. The asymmetry of the forelimb usage was expressed as "limb-use symmetry ratio" – independent contralateral (to the lesion) paw placement relative to that of the ipsilateral paw against the walls of the chamber during rearing and vertical/lateral explorations.

### Serotonin depletion in mice

Serotonin depletions were produced in mice of the same age with three daily injections of 300 mg/kg 4-chloro-DL-phenylalanine methyl ester hydrochloride. These mice were killed for experiments 24 h after the final injection.

### Slice preparation

Mice were anesthetized before decapitation. The brain was rapidly removed, and a block containing the GPe and surrounding structures was dissected out, attached to a mounting tray with cyanoacrylate glue, and immersed in ice-cold ACSF consisting of the following (in mM): 125 NaCl, 25 $NaHCO_3$, 2.5 KCl, 1.25 $NaH_2PO_4$*$H_2O$, 1 $MgCl_2$*$6H_2O$, 2 $CaCl_2$*$2H_2O$, 13 glucose and saturated with carbogen (95% $O_2$ and 5% $CO_2$). 250 μm parasagittal slices were cut using a vibrating microtome (Leica Instrument). Slices were transferred to fresh ACSF and equilibrated at 34 °C for 30 min, and then maintained at room temperature (~22 °C) for at least 30 minutes prior to electrophysiological recording and acute dissociation.

### Visualized recording *in vitro*

Slices were transferred to a recording chamber that was mounted on a fixed-stage, upright microscope (Olympus) equipped with infrared differential interference contrast (IR-DIC) optics. The recording chamber was superfused with carbogen-saturated ACSF with a flow rate of 2–3 ml/min. Experiments were performed at room temperature. Patch electrodes had resistance of 3–5 MΩ when filled with an internal solution consisting of the following (mM): 140 $KMeSO_4$, 10 KCl, 10 HEPES, 2 $Mg_2ATP$, and 0.4 $Na_3GTP$, 10 Na-phosphocreatine and 0.2% biocytin; pH adjusted to 7.25 with KOH. Recordings were made with a Multiclamp 700B amplifier (Molecular Devices) operating in either current-clamp or voltage-clamp mode on the soma of GPe neurons. Electrophysiological records were acquired at 5 or 10 kHz with a Digidata 1322A interface (Molecular Devices) in conjunction

Author Manuscript Author Manuscript Author Manuscript Author Manuscript

with a PC, and filtered at 1 or 2 kHz, respectively, with a low pass Bessel filter. Stimulus generation and data acquisition was performed using pClamp9 (Molecular Devices).

### Two-photon $Ca^{2+}$ imaging

GPe neurons in tissue slices(as described above) were loaded with Alexa Fluor 594 (50 μM)and Fluo-4 (200 μM) through the patch pipette. All experimentswere performed at room temperature. Images were acquired witha 60×/1.00 NA water-immersion lens (Olympus). The two-photon excitationsource was a Chameleon-ultra2 tunable laser system (680 to 1080nm) using titanium:sapphire gain medium with all-solid-stateactive components and a computer-optimized algorithm to ensurereproducible excitation wavelength, average power, and peakpower (Coherent Laser Group). Optical signals were acquiredusing 810 nm excitation beam (80-MHz pulse repetition frequencyand 250 fs pulse duration) to simultaneously excite Alexa andFluo-4. The fluorescence emission was collectedby external or non-descanned photomultiplier tubes (PMTs). Thegreen fluorescence (500–550 nm) was detected by a bialkali-cathodePMT, and the red fluorescence (580–640 nm) was collectedby a multi-alkali-cathode (S-20) PMT. Measurements weretaken in a sample plane along dendritic segments (100–150 μm from the soma). Line scan signals were acquired (as described above) at 6 ms per line with 0.18 μmpixels and 10 μs pixel dwell time. The time between thecontrol and isradipine treatment measurements was 5–7min.

### *In vivo* unit recording and local injection of drugs in rats

The rats were anesthetized with a mixture of ketamine and xylazine, mounted on a stereotaxic apparatus and the skull exposed. A plastic recording chamber, which also function as a device to fix their heads painlessly to a stereotaxic frame, was placed on the skull and secured with dental acrylic. A small hole was drilled in the skull over the lateral agranular cortex and a parallel bipolar stimulus electrode (100 μm insulated stainless steel wires) was implanted. Another hole was drilled into the skull over the GPe and the STN for recording electrode penetration. After recovery form the surgery, rats were anesthetized with isoflurane and mounted on a stereotaxic device using a plastic head holder on the skull. Rats were maintained with 0.5–1.0% isoflurane during the recording session. Single-unit recordings of GPe neurons were made with insulated tungsten electrodes (AC resistance 1–2 MΩ), amplified, passed through a 0.7–2 kHz band-pass filter, and then to a homemade window discriminator. A glass micropipette with a tip diameter of less than 50 μm that was glued to the needle of the 10 μl Hamilton syringe filled with muscimol (0.5 μg/μl saline) and multi-unit recordings were made.

### HCN2 transgene expression and electrophysiological analyses

A recombinant adeno-associated virus (AAV2 serotype) based two-vector system was used. The activator vector consisted of a glutamate decarboxylase 1 (GAD1) promoter driving expression of a tetracycline transactivator protein (tTA); the responder vector consisted of a tTA regulated tet-operator-CMV (tetO-CMV) bidirectional promoter driving coexpression of HCN2 and eGFP. Expression from the responder vector is activated only in the presence of the activator vector expressing tTA (i.e. HCN2 expression reported by eGFP-fluorescence was achieved by co-infection of GPe neurons with the responder and activator viruses). AAVs were produced by The Gene Therapy Program of the University of Pennsylvania. A

Author Manuscript Author Manuscript Author Manuscript Author Manuscript

mixture of activator and responder viruses were injected into the GPe using standard procedures three weeks after behavioral characterization of 6-OHDA lesioned mice/rats. Recordings were made 2–5 weeks after viral injections. For *in vitro* experiments, only weak to moderately eGFP-positive neurons along with non-infected controls were selected for electrophysiological analyses.

### Real-time PCR quantification

In brief, 250 μm coronal slices containing GPe were microdissected. Total RNA was isolated using TRIzol (Invitrogen) according to the manufacturer's instructions. RNA samples were treated with DNase I (Ambion) to eliminate genomic DNA contamination, and cDNA was synthesized using qScript cDNA Supermix (Quanta Biosciences). Real-time PCR was performed using SYBR Green I on a StepOnePlus thermocycler (Applied Biosystems). The thermal cycling conditions composed of an initial denaturing step at 95 °C for 3 min, and 40 cycles at 95 °C for 15 s, 60 °C for 60 s, and 72 °C for 30 s. The PCR cycle threshold ($C_T$) values were measured within the exponential phase of the PCR reaction using StepOnePlus (Applied Biosystems). A relative quantification method (i.e. $-\Delta\Delta C_T$ method) was used to quantify difference in gene expression level by comparison with GAPDH, an endogenous reference gene. Experiments for each gene of interest were run in triplicate. Desalted primers were custom-synthesized (Invitrogen) and intron-spanning. The gene expression levels in each sample were characterized by their median values and ranges, standard error of the mean of individual reactions, and their coefficients of variation. Results were presented as fold difference relative to whole brain. Statistical analysis (Mann-Whitney *U*-test) was performed. Differences between the cell groups were judged significant at confidence levels of 95% ($P < 0.05$).

### Western Blot analyses

Tissue dissection and harvesting were performed as described above. Membrane protein fractions were prepared by lysis of tissue in buffer containing 10 mM HEPES, pH 7.4, and 320 mM sucrose, followed by brief centrifugation to remove nuclei and insoluble material. After centrifugation at 16,000× *g*, the pellet was resuspended by gentle rocking at 4 °C in TEEN-Tx (0.1 M Tris, 1 mM EDTA, 1 mM EGTA, and 1% Triton X-100). Protein extracts were resolved by SDS-PAGE, and transferred to polyvinylidene difluoride membranes. Western blotting was performed using the following primary antibodies as previously described [27], [29]: anti-HCN1, 1:2,000, anti-HCN2, 1:2,000, anti-HCN3, 1:500, anti-HCN4, 1:2,000, anti-TRIP8b, 1:5,000, and anti-α-tubulin, 1:10,000 (Upstate Biotechnology). Densitometric quantification of signal intensity was performed using NIH ImageJ software, and α-tubulin signal intensity was used as a loading control.

### Behavioral testing

Behaviroal procedures and parameters were similar to those previously described [45]. Stepping Test: Mice were held by the tail with their hindlimbs suspended above the table and dragged backwards at a steady rate for 1 m over 3–4 s. Number of adjusting steps made with the contralateral or ipsilateral paw relative to the lesioned hemisphere was recorded [46]. Pole Test: Mice were placed facing upwards on a wooden pole (50 cm long and 1 cm in

Author Manuscript Author Manuscript Author Manuscript Author Manuscript

diameter) that leads into their home cage. Mice were trained and assessed. Turning time and total time to descend were recorded. Adhesive Removal: Adhesive dots (0.6 cm diameter) were placed on the either side of the nose of the mouse and the time to remove the dots was recorded. Gait analysis: Mice were trained to traverse a path leading to the home cage mouse. Following training, hindpaws were dipped in non-toxic paint to record paw prints of the animals. Average stride length was measured using only steps where the animal was continuously walking at a regular pace. Challenge Beam Task: Mice were trained to traverse a plexiglass beam of decreasing width with an overhang ledge on both sides of the beam and a wire grid placed on top of the beam. The time to traverse the beam, total number of steps, and total number of errors were assessed. Spontaneous Activity (Cylinder Task): Spontaneous behavior was evaluated by monitoring movement in a transparent cylinder (15.5 cm in height and 12.7 cm in diameter) for 3 minutes. The cylinder was placed on a piece of glass and a mirror was place below the cylinder to visualize stepping movement from underneath. Number of steps taken by the contralateral and ipsilateral paws, total rearing movements, and total time spent grooming were evaluated.

### Data analysis and statistics

Curve-fitting, data and statistical analyses, and plotting were done using Clampfit9 (Molecular Devices) and IgorPro 6.0 (WaveMetrics, Lake Oswego, OR). Data were presented as median or mean ± s.e.m., and compared statistically using Mann-Whitney rank sum test. Kolmogorov-Smirnov test was used to compare distributions of datasets. P values $< 0.05$ indicate statistical significance.

## Supplementary Material

Refer to Web version on PubMed Central for supplementary material.

## Acknowledgments

The authors thank Yu Chen, Karen Saporito, and Sasha Ulrich for technical assistance. This work was supported by Parkinson's disease foundation and American Parkinson Disease Association Research to C.S.C.; Michael J. Fox foundation to P.O.; Hartmann Foundation to D.J.S.; National Institutes of Health grants NS069777 to C.S.C, MH082522 to T.S.G., NS064757 to A.S.L., NS05595 and NS059934 to D.M.C., NS042762 to H.K. and NS047085 to D.J.S.

## References

1. DeLong MR, Wichmann T. Circuits and circuit disorders of the basal ganglia. Arch Neurol. 2007; 64:20–24. [PubMed: 17210805]
2. Hammond C, Bergman H, Brown P. Pathological synchronization in Parkinson's disease: networks, models and treatments. Trends Neurosci. 2007; 30:357–364. [PubMed: 17532060]
3. Rivlin-Etzion M, et al. Basal ganglia oscillations and pathophysiology of movement disorders. Curr Opin Neurobiol. 2006; 16:629–637. [PubMed: 17084615]
4. Graybiel AM. Habits, rituals, and the evaluative brain. Annu Rev Neurosci. 2008; 31:359–387. [PubMed: 18558860]
5. DeLong MR. Activity of pallidal neurons during movement. J Neurophysiol. 1971; 34:414–427. [PubMed: 4997823]
6. Chan CS, Shigemoto R, Mercer JN, Surmeier DJ. HCN2 and HCN1 channels govern the regularity of autonomous pacemaking and synaptic resetting in globus pallidus neurons. J Neurosci. 2004; 24:9921–9932. [PubMed: 15525777]

Author Manuscript Author Manuscript Author Manuscript Author Manuscript

7. Stanford IM. Independent neuronal oscillators of the rat globus pallidus. Journal of neurophysiology. 2003; 89:1713–1717. [PubMed: 12626634]
8. Kita H, Kitai ST. Intracellular study of rat globus pallidus neurons: membrane properties and responses to neostriatal, subthalamic and nigral stimulation. Brain Res. 1991; 564:296–305. [PubMed: 1810628]
9. Nambu A, Llinas R. Electrophysiology of globus pallidus neurons in vitro. Journal of neurophysiology. 1994; 72:1127–1139. [PubMed: 7807199]
10. Bevan MD, Magill PJ, Terman D, Bolam JP, Wilson CJ. Move to the rhythm: oscillations in the subthalamic nucleus-external globus pallidus network. Trends Neurosci. 2002; 25:525–531. [PubMed: 12220881]
11. Obeso JA, et al. Pathophysiology of the basal ganglia in Parkinson's disease. Trends Neurosci. 2000; 23:S8–19. [PubMed: 11052215]
12. Walters JR, Ruskin DN, Allers KA, Bergstrom DA. Pre- and postsynaptic aspects of dopamine-mediated transmission. Trends Neurosci. 2000; 23:S41–47. [PubMed: 11052219]
13. Mallet N, Ballion B, Le Moine C, Gonon F. Cortical inputs and GABA interneurons imbalance projection neurons in the striatum of parkinsonian rats. J Neurosci. 2006; 26:3875–3884. [PubMed: 16597742]
14. Terman D, Rubin JE, Yew AC, Wilson CJ. Activity patterns in a model for the subthalamopallidal network of the basal ganglia. J Neurosci. 2002; 22:2963–2976. [PubMed: 11923461]
15. Gillies A, Willshaw D, Li Z. Subthalamic-pallidal interactions are critical in determining normal and abnormal functioning of the basal ganglia. Proc Biol Sci. 2002; 269:545–551. [PubMed: 11916469]
16. Surmeier DJ, Mercer JN, Chan CS. Autonomous pacemakers in the basal ganglia: who needs excitatory synapses anyway? Curr Opin Neurobiol. 2005; 15:312–318. [PubMed: 15916893]
17. Mercer JN, Chan CS, Tkatch T, Held J, Surmeier DJ. Nav1.6 sodium channels are critical to pacemaking and fast spiking in globus pallidus neurons. J Neurosci. 2007; 27:13552–13566. [PubMed: 18057213]
18. Zhang W, Linden DJ. The other side of the engram: experience-driven changes in neuronal intrinsic excitability. Nat Rev Neurosci. 2003; 4:885–900. [PubMed: 14595400]
19. Turrigiano GG, Nelson SB. Homeostatic plasticity in the developing nervous system. Nat Rev Neurosci. 2004; 5:97–107. [PubMed: 14735113]
20. Iancu R, Mohapel P, Brundin P, Paul G. Behavioral characterization of a unilateral 6-OHDA-lesion model of Parkinson's disease in mice. Behavioural brain research. 2005; 162:1–10. [PubMed: 15922062]
21. Schallert T, Fleming SM, Leasure JL, Tillerson JL, Bland ST. CNS plasticity and assessment of forelimb sensorimotor outcome in unilateral rat models of stroke, cortical ablation, parkinsonism and spinal cord injury. Neuropharmacology. 2000; 39:777–787. [PubMed: 10699444]
22. Albin RL, Young AB, Penney JB. The functional anatomy of basal ganglia disorders. Trends Neurosci. 1989; 12:366–375. [PubMed: 2479133]
23. Shin RM, et al. Dopamine D4 receptor-induced postsynaptic inhibition of GABAergic currents in mouse globus pallidus neurons. J Neurosci. 2003; 23:11662–11672. [PubMed: 14684868]
24. Cooper AJ, Stanford IM. Dopamine D2 receptor mediated presynaptic inhibition of striatopallidal GABA(A) IPSCs in vitro. Neuropharmacology. 2001; 41:62–71. [PubMed: 11445186]
25. Chan CS, et al. 'Rejuvenation' protects neurons in mouse models of Parkinson's disease. Nature. 2007; 447:1081–1086. [PubMed: 17558391]
26. Biel M, Wahl-Schott C, Michalakis S, Zong X. Hyperpolarization-activated cation channels: from genes to function. Physiol Rev. 2009; 89:847–885. [PubMed: 19584315]
27. Lewis AS, et al. Alternatively spliced isoforms of TRIP8b differentially control h channel trafficking and function. J Neurosci. 2009; 29:6250–6265. [PubMed: 19439603]
28. Santoro B, Wainger BJ, Siegelbaum SA. Regulation of HCN channel surface expression by a novel C-terminal protein-protein interaction. J Neurosci. 2004; 24:10750–10762. [PubMed: 15564593]
29. Notomi T, Shigemoto R. Immunohistochemical localization of Ih channel subunits, HCN1-4, in the rat brain. The Journal of comparative neurology. 2004; 471:241–276. [PubMed: 14991560]

Author Manuscript Author Manuscript Author Manuscript Author Manuscript

30. Chung WK, et al. Absence epilepsy in apathetic, a spontaneous mutant mouse lacking the h channel subunit, HCN2. Neurobiol Dis. 2009; 33:499–508. [PubMed: 19150498]
31. Nolan MF, et al. The hyperpolarization-activated HCN1 channel is important for motor learning and neuronal integration by cerebellar Purkinje cells. Cell. 2003; 115:551–564. [PubMed: 14651847]
32. Galati S, et al. The pharmacological blockade of medial forebrain bundle induces an acute pathological synchronization of the cortico-subthalamic nucleus-globus pallidus pathway. J Physiol. 2009; 587:4405–4423. [PubMed: 19622605]
33. Heimer G, Bar-Gad I, Goldberg JA, Bergman H. Dopamine replacement therapy reverses abnormal synchronization of pallidal neurons in the 1-methyl-4-phenyl-1,2,3,6-tetrahydropyridine primate model of parkinsonism. J Neurosci. 2002; 22:7850–7855. [PubMed: 12223537]
34. Walters JR, Hu D, Itoga CA, Parr-Brownlie LC, Bergstrom DA. Phase relationships support a role for coordinated activity in the indirect pathway in organizing slow oscillations in basal ganglia output after loss of dopamine. Neuroscience. 2007; 144:762–776. [PubMed: 17112675]
35. Mallet N, et al. Parkinsonian beta oscillations in the external globus pallidus and their relationship with subthalamic nucleus activity. J Neurosci. 2008; 28:14245–14258. [PubMed: 19109506]
36. Shah MM, Anderson AE, Leung V, Lin X, Johnston D. Seizure-induced plasticity of h channels in entorhinal cortical layer III pyramidal neurons. Neuron. 2004; 44:495–508. [PubMed: 15504329]
37. Strauss U, et al. An impaired neocortical Ih is associated with enhanced excitability and absence epilepsy. Eur J Neurosci. 2004; 19:3048–3058. [PubMed: 15182313]
38. Kole MH, Brauer AU, Stuart GJ. Inherited cortical HCN1 channel loss amplifies dendritic calcium electrogenesis and burst firing in a rat absence epilepsy model. J Physiol. 2007; 578:507–525. [PubMed: 17095562]
39. Destexhe A, Marder E. Plasticity in single neuron and circuit computations. Nature. 2004; 431:789–795. [PubMed: 15483600]
40. Zucker RS. Calcium- and activity-dependent synaptic plasticity. Curr Opin Neurobiol. 1999; 9:305–313. [PubMed: 10395573]
41. Xu W, Lipscombe D. Neuronal Ca(V)1.3alpha(1) L-type channels activate at relatively hyperpolarized membrane potentials and are incompletely inhibited by dihydropyridines. J Neurosci. 2001; 21:5944–5951. [PubMed: 11487617]
42. Robinson RB, Siegelbaum SA. Hyperpolarization-activated cation currents: from molecules to physiological function. Annu Rev Physiol. 2003; 65:453–480. [PubMed: 12471170]
43. Hernandez A, et al. Control of the subthalamic innervation of the rat globus pallidus by D2/3 and D4 dopamine receptors. Journal of neurophysiology. 2006; 96:2877–2888. [PubMed: 16899633]
44. Higley MJ, Sabatini BL. Competitive regulation of synaptic Ca(2+) influx by D2 dopamine and A2A adenosine receptors. Nature neuroscience. 2010
45. Fleming SM, et al. Early and progressive sensorimotor anomalies in mice overexpressing wild-type human alpha-synuclein. J Neurosci. 2004; 24:9434–9440. [PubMed: 15496679]
46. Blume SR, Cass DK, Tseng KY. Stepping test in mice: a reliable approach in determining forelimb akinesia in MPTP-induced Parkinsonism. Experimental neurology. 2009; 219:208–211. [PubMed: 19460369]

Author Manuscript Author Manuscript Author Manuscript Author Manuscript

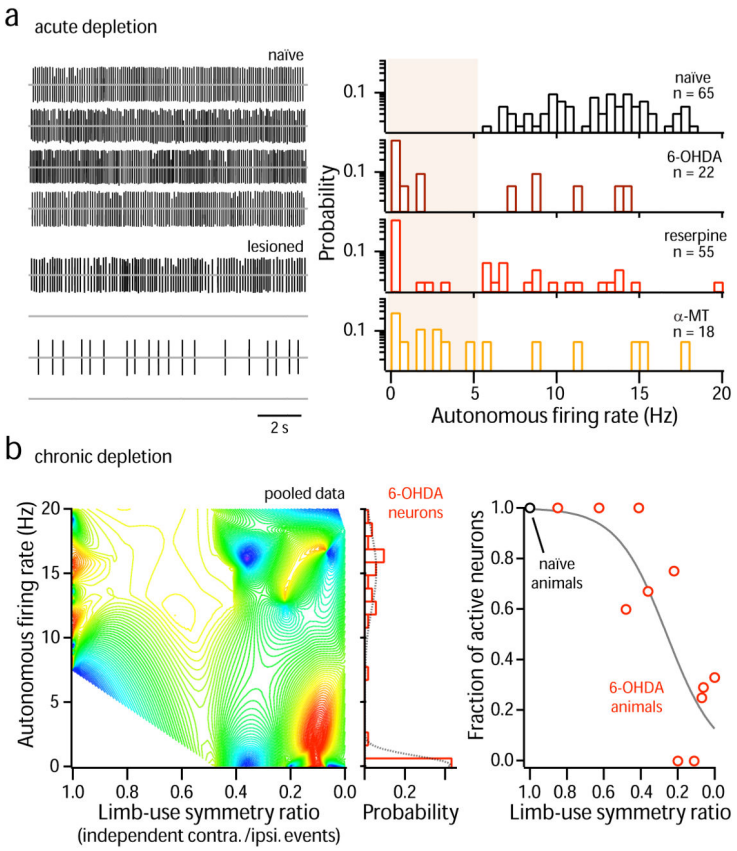


**Figure 1.**

Dopamine depletion reduces autonomous activity of GPe neurons. (**a**) Representative cell-attached recordings of naïve and 6-OHDA lesioned cells. To the right, histogram of discharge rates from naïve and various dopamine depleting conditions. (**b**) Discharge rate vs. limb asymmetry in the animal from which the neuron was taken; number of observations is denoted by temperature of colors. The same set of data from 6-OHDA animals was also presented in histogram format. Note that the response of GPe neurons to dopamine depletion is bimodal. Limb-use symmetry ratio of naïve animals was assumed to be one. (**c**) Plot of the fraction of active neurons as a function of limb asymmetry following 6-OHDA lesions.

Author Manuscript Author Manuscript Author Manuscript Author Manuscript

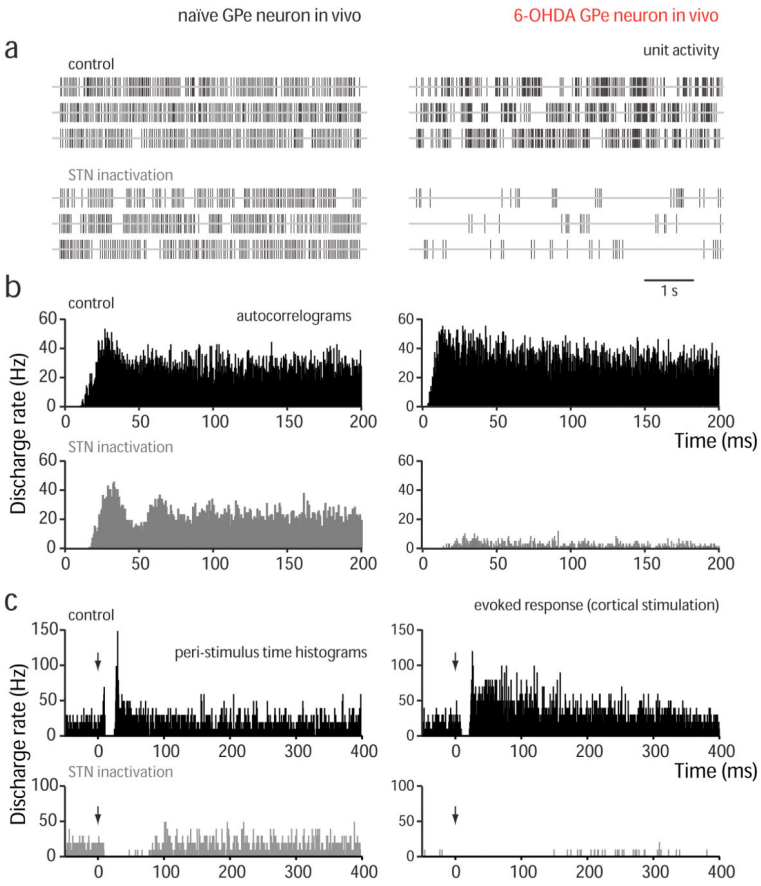


**Figure 2.**

Spontaneous activity of GPe neurons from chronic dopamine depletion *in vivo*. (**a**) Unit activity recordings of GPe neurons from before and after muscimol injection (0.5 μg/μl, total injection volume of 0.1 μl) into the STN. In control rats, the rate firing decreased from 44.1 ± 11.8 to 25.2 ± 9.9 (n = 8), compared immediately before injection and 15 min after the injection. In 6-OHDA treated rats, muscimol silenced the firing activity of GPe neurons within a few min (38.2 ± 14.8 to 0, n = 9). No spontaneously active neurons could be found in the GPe of the same electrode track. (**b**) autocorrelograms of unit activity from various conditions. (**c**) Peri-stimulus time histogram (PSTH) of cortical stimulation induced responses in the GPe. Cortical stimulation (arrow) evoked combinations of early excitation, inhibition, and late excitation in GPe neurons.

Author Manuscript Author Manuscript Author Manuscript Author Manuscript

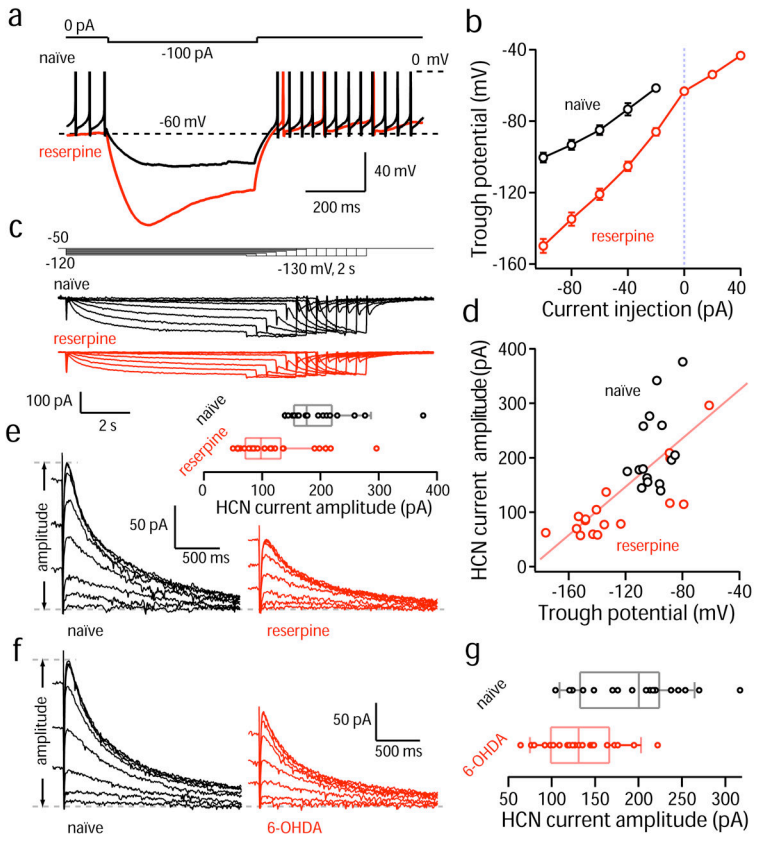


**Figure 3.**

Diminished HCN channel activity in GPe neurons following acute and chronic dopamine depletion. (**a**) Membrane response of GPe neurons from naïve and dopamine depleted animals. (**b**) Summary of the membrane response of GPe neurons to a series of current injections. Note the discontinuity (dotted line) of the membrane response from −60 mV and below from reserpine-treated group. For clarity purposes, only silent neurons from the reserpine-treated animals were included. Numerical data are expressed as mean ± s.e.m. (**c**) Top, voltage clamp records of HCN currents from control and dopamine depleted animals. Note the reduction in size of the HCN current amplitude following dopamine depletion ($P<0.05$, Mann-Whitney). Bottom, summary of voltage deflection vs. current amplitude in control and dopamine depleted animals. The five reserpine-treated neurons with HCN current amplitudes greater than 180 pA were spontaneously active. (**d**) Relationship between voltage deflection and HCN amplitude (correlation coefficient = 0.78, $P<0.001$, Spearman rank correlation). (**e**) Tail currents from control and reserpinized cells. Fitting the current-voltage relationship of the HCN channel with a Boltzmann function reveals no difference ($P>0.05$, Mann-Whitney) in the voltage dependence of activation (median: naïve= −90.2 mV, n = 5; reserpine= −87.4 mV, n = 12). (**f**) Records similar to **e** but from 6-OHDA lesioned animals. (**g**) Summary showing reduction of HCN current amplitudes in GPe cells from control and 6-OHDA lesioned mice ($P<0.05$, Mann-Whitney). In data presented as box plots, the central line represents the median, the edges of the box represents the interquartile range, and the “whisker lines” show the extent of the overall distribution.

Author Manuscript Author Manuscript Author Manuscript Author Manuscript

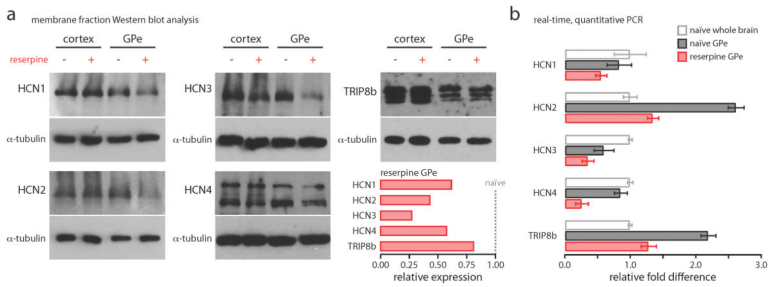


**Figure 4.**

Western blot and qPCR analysis of HCN channel subunits. (**a**) Membrane-bound protein expression of HCN1–4 and Trip8b in the GPe and the adjacent cortex from naïve and dopamine depleted mice. α-tubulin was used as the loading control. Quantification of change in the GPe following reserpine treatment is summarized on the bottom right. Dotted line indicates control levels from naïve animals. (**b**) qPCR expression analysis HCN1–4 and Trip8b in GPe relative to whole brain. Note the enrichment of HCN2 subunits in naïve GPe (>1). A global downregulation of all α-subunits and TRIP8b was observed.

Author Manuscript Author Manuscript Author Manuscript Author Manuscript

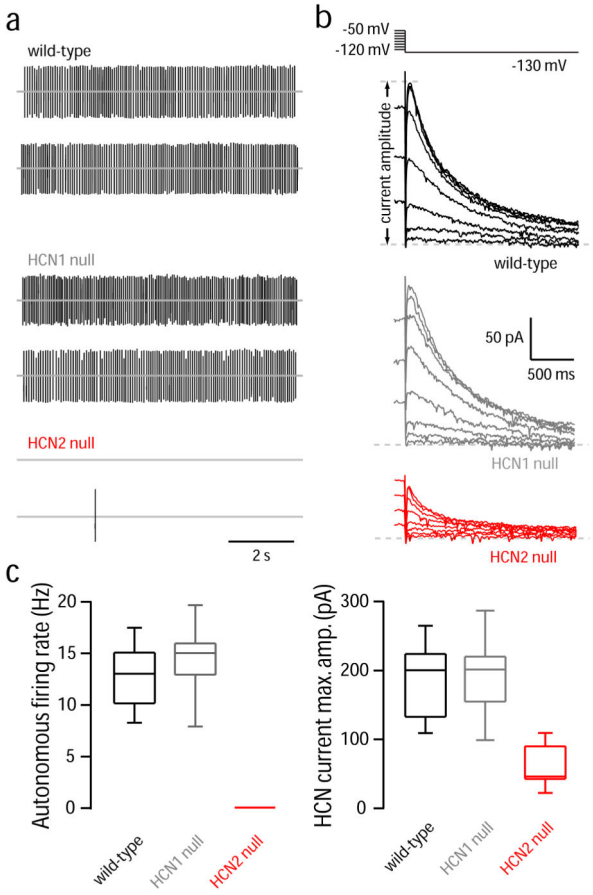


**Figure 5.**

Autonomous activity and HCN currents of GPe neurons from mice lacking HCN1 or HCN2. (**a**) Representative cell-attached recordings in wild-type mice and mice lacking HCN1 or HCN2. Note GPe neuron activity from HCN1 null mice (n = 14, P>0.05, Mann-Whitney) was similar to that seen in wild-type (n = 131), while that from the HCN2 null mice were quiescent (n = 15). (**b**) Representative cell-attached recordings and tail current recordings in wild-type mice and mice lacking HCN1 or HCN2. Note HCN currents from GPe neurons from *Hcn1*$^{-/-}$ mice (n = 9) were largely similar to that of wild-type (n = 50, P>0.05, Mann-Whitney), while that from the HCN2 null mice (n = 15, P<0.05, Mann-Whitney) were dramatically reduced. (**c**) Summary data showing the autonomous discharge and HCN current amplitude in GPe neurons from wild-type and subunit-specific mutant mice.

Author Manuscript Author Manuscript Author Manuscript Author Manuscript

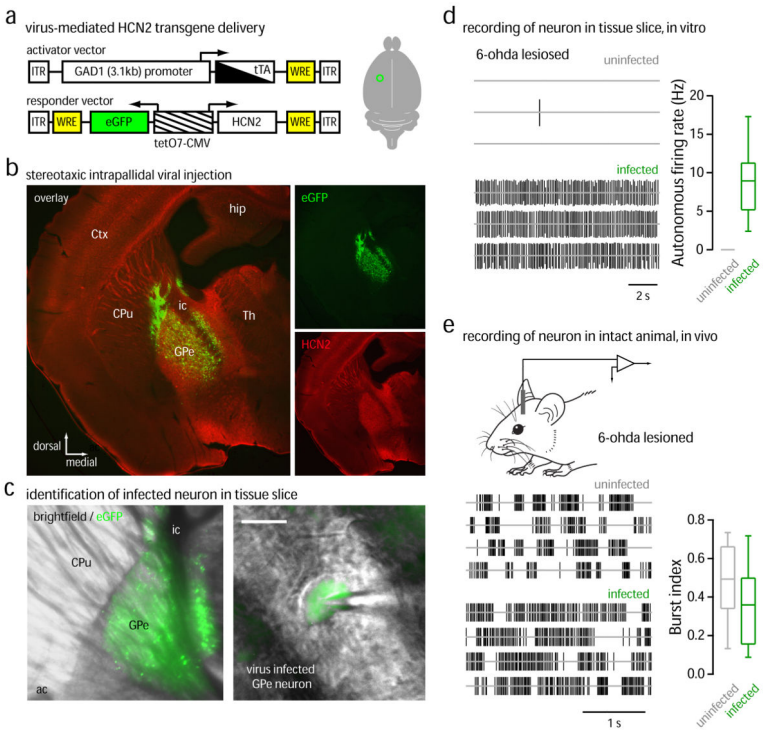


**Figure 6.**

Recombinant AAV-mediated HCN2 subunit delivery in GPe. (**a**) Schematic of regulated expression constructs and injection site. (**b**) Photomicrograph of a mouse coronal brain section demonstrating AAV infection (eGFP fluorescence) with stereotaxic intrapallidal injection. (**c**) Identification of AAV infection in GPe tissue slice (left) and in a GPe neuron (right). (**d**) Representative *in vitro* cell-attached recordings in uninfected (n = 5) and infected neurons. Rescue of autonomous activity in GPe neurons was observed in a majority of infected neurons (9 out of 15). Right, data were summarized on the right in box plot format. For clarity purposes, only active neurons from the infected group were presented. Right, the burst index of neurons were quantified. (**e**) Representative *in vivo* recordings in 6-OHDA lesion rats before and after AAV infection. Reduction of burst firing in GPe neurons was evident. Right, data were summarized on the right in box plot format. Abbreviations: caudate putamen (CPu), cortex (Ctx), hippocampus (Hip), thalamus (Th), anterior commisure (ac) and internal capsule (ic). Scale bar: 20 μm.

Author Manuscript Author Manuscript Author Manuscript Author Manuscript

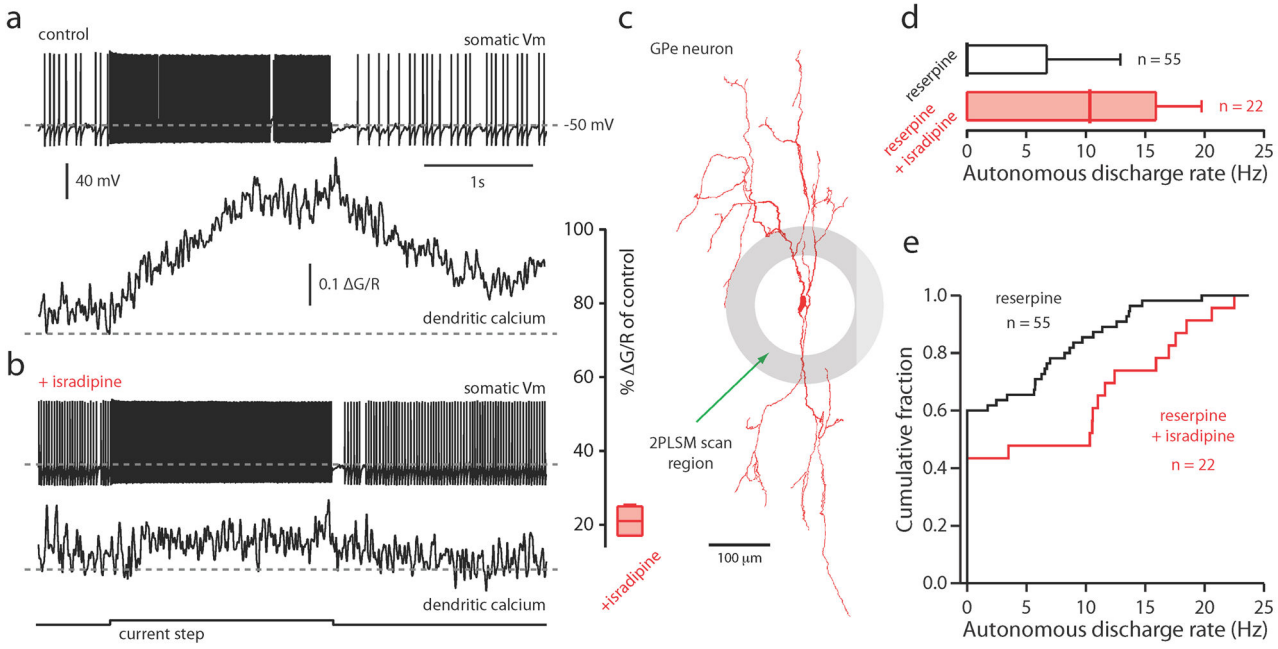


**Figure 7.**

Cellular activity appeared to be encoded by $Ca^{2+}$ influx via Cav1/L-type $Ca^{2+}$ channels in GPe neurons. (**a–c**) Burst firing induced $Ca^{2+}$ influx in GPe neuron dendrites via Cav1/L-type $Ca^{2+}$ channel. Antagonism of L-type channels in GPe neurons attenuated $Ca^{2+}$ transients associated with spike bursts. Top (**a**) and bottom (**b**) panels show recordings from a pacemaking GPe neuron before and after a depolarizing current (80 pA) step (2 s) while imaging dendritic $Ca^{2+}$ approximately 100 microns away from soma (**c**). Current injection induced a robust $Ca^{2+}$ influx that was sensitive to antagonism of L-type channels (5 µM isradipine). The extent of the reduction in $Ca^{2+}$ signal was calculated by measuring the change in the G/R ratio before and after bursting. Right, box plot summarizes four GPe neurons in which the burst response was measured before and after isradipine application; responses were reduced by roughly 80%. (**d–e**) Cav1/L-type $Ca^{2+}$ channel antagonism attenuate silencing in GPe neurons. Box plot (**d**) showing sparing of activity of GPe neurons from isradipine-treated mouse (red). Data are summarized as a cumulative plot (**e**).